ISSN 0036-0236, Russian Journal of Inorganic Chemistry, 2024. © Pleiades Publishing, Ltd., 2024.

PHYSICOCHEMICAL ANALYSIS OF INORGANIC SYSTEMS

Subsolidus Phase Equilibria in the La_2O_3–(Ni/Co)O–Sb_2O_5 Systems

A. V. Egorysheva[a, *], S. V. Golodukhina[a], K. R. Plukchi[a, b], L. S. Razvorotneva[a, c], A. V. Khoroshilov[a], and O. G. Ellert[a]

[a] *Kurnakov Institute of General and Inorganic Chemistry, Russian Academy of Sciences, Moscow, 119991 Russia*

[b] *Faculty of Materials Science, Moscow State University, Moscow, 119991 Russia*

[c] *National Research University Higher School of Economics, Moscow, 101000 Russia*

**e-mail: anna_egorysheva@rambler.ru*

Received March 21, 2024; revised April 2, 2024; accepted April 4, 2024

Abstract—Subsolidus phase equilibria in the La_2O_3–(Ni/Co)O–Sb_2O_5 systems have been studied. A previously unknown compound $La_4Sb_2O_{11}$ was found to exist in the La_2O_3–Sb_2O_5 system. $La_4Sb_2O_{11}$ has been shown to decompose at 1060°C to form La_3SbO_7 and $LaSbO_4$. Two ternary oxides ($LaNi_2SbO_6$ and $La_2NiSb_2O_9$) have been discovered in the La_2O_3–NiO–Sb_2O_5 system. These new compounds are stable and do not undergo polymorphic transformations throughout the range of temperatures studied (25–1350°C). The existence of previously known ternary oxides, namely perovskite $La_3Ni_2SbO_9$ and rosiaite $LaNi_{1/3}Sb_{5/3}O_6$, has been verified. In the La_2O_3–CoO–Sb_2O_5 system, two new compounds ($LaCo_2SbO_6$ and $La_2CoSb_2O_9$) have been found along with previously known perovskite $La_3Co_2SbO_9$, rosiaite $LaCo_{1/3}Sb_{5/3}O_6$, and rhombohedral pyrochlore $La_3Co_2Sb_3O_{14}$. These new compounds are isostructural to those found in the nickel oxide system. $La_2CoSb_2O_9$, unlike its nickel analogue, decomposes at 990°C. For $LaCo_2SbO_6$, no thermal events associated with polymorphic transitions or melting have been detected on DSC curves up to 1350°C. An inspection of diffuse reflectance spectra of the newly synthesized $LaNi_2SbO_6$, $La_2NiSb_2O_9$, $LaCo_2SbO_6$, and $La_2CoSb_2O_9$ phases showed that the oxidation state of nickel and cobalt in them is 2+. The 1050°C isothermal sections of La_2O_3–(Ni/Co)O–Sb_2O_5 systems have been constructed.

Keywords: phase equilibria, antimonates, nickel oxides, cobalt oxides

DOI: 10.1134/S0036023624601107

INTRODUCTION

Phase equilibria in multicomponent systems are directly related to the search for new functional materials based on complex oxides and the development of optimal methods for their synthesis. Despite an enormous amount of research work carried out to date into phase equilibria in binary and multicomponent oxide systems, a great many of the systems remain poorly studied. Such are systems comprising antinomy oxide, whose high volatility makes investigations difficult. Meanwhile, many promising functional materials, in particular catalysts, have been created based on antimonates. Various M–Sb–O double oxides (where M = Mg, Ca, Sr, Al, Cr, Fe, Co, Ni, Cu, Zn, Y, Ag, In, La, Pb, or Bi) have shown their efficacy in photocatalytic water splitting [1–8]. Transition-metal antimonates MSb_2O_6, where M = Mn, Fe, Co, and Ni, have been used as low-cost (free of precious metals) catalysts, which are distinguished by their good oxygen binding energy, conductivity, thermal phase stability, and stability in aqueous media. These catalysts can be used in the electrocatalytic reduction of oxygen [3–7] and for the electrochemical release of chlorine [2, 6]. The reason for the catalytic activity of antimonates in redox reactions is the low redox potential of the $Sb^{3+} \rightarrow Sb^{5+}$ transformations [9]. It is due to this feature that iron antimonate $FeSbO_4$ is an efficient oxidation catalyst in various organic syntheses [10–13]. We showed recently [14–20] that pyrochlore ternary oxides $(Ln_{1.8}Fe_{0.2})FeSbO_7$ (Ln = Pr–Tb, or Bi) and rosiaites $LnFe_{0.5}Sb_{1.5}O_6$ (Ln = La–Sm) and $LaNi_{1/3}Sb_{5/3}O_6$ exhibit high activity and stability in catalytic CO oxidation and complete methane oxidation.

The study of phase equilibria in antimony-containing multicomponent oxide systems will elucidate previously unknown phases and, possibly, expand the range of promising antimonate-based functional materials. In particular, of interest are La_2O_3–(Ni/Co)O–Sb_2O_5 systems, which have not been studied but the boundary binary systems of which have been in sufficient detail.

In the Ni–Sb–O system, only two mixed oxides exist: $NiSb_2O_4$ and $NiSb_2O_6$ [21]. $NiSb_2O_6$ has the trirutile structure (space group $P4_2/mnm$) [22, 23]; it is stable in air (at least to 1523°C) and can be used in C_3H_8 and CO sensors [24] and liquefied petroleum gas sensors [25]. $NiSb_2O_6$ has a metastable rosiaite-type

polymorph (space group $P\bar{3}1m$) [26] with the unit cell parameters a = 4.691(7) Å, c = 9.299(3) Å. When heated for more than 1 h at 500°C, however, this compound transforms to a stable phase. $NiSb_2O_4$ belongs to the Pb_3O_4 structure type (space group $P4_2/mbc$) [27] and can be prepared only via heating NiO and Sb_2O_3 mixtures in vacuo or in flowing nitrogen [21].

In the Co–Sb–O system, as in the nickel system, there is a trirutile phase [28]. Also known are spinel $Co_{7/3}Sb_{2/3}O_4$ (space group $Fd\bar{3}m$) [29] and pyrochlore $Co_2Sb_2O_7$ (space group $Fd\bar{3}m$) [30, 31]. A $Co_{7/3}Sb_{2/3}O_4$ phase was prepared from cobalt sulfate and antimony oxide (Sb_2O_3) by annealing at 900°C; $Co_2Sb_2O_7$ was prepared from cobalt acetate and antimony oxide (Sb_2O_5) at 450°C, but it is yet unknown whether this phase is stable at high temperatures.

The La–Ni–O system was studied in detail at 1200°C [32]. Under air, the system can form $LaNiO_3$ and Ruddlesden–Popper homologous phases of general formula $La_{n+1}Ni_nO_{3n+1}$ (n is the number of octahedral layers) [33]: La_2NiO_4, $La_3Ni_2O_7$, and $La_4Ni_3O_{10}$. Their crystal lattices are formed by the alternation of perovskite layers and NaCl-type layers. $LaNiO_3$ has the perovskite structure [34]; it is stable below 850°C in air or under an elevated oxygen pressure. Above 850°C, this phase gradually decomposes to $La_{n+1}Ni_nO_{3n+1}$ oxides [32, 33, 35]. According to Kitayama [32], an $La_6Ni_5O_{15}$ phase exists; it was prepared at 1200°C under air. According to Demina at el. [36], however, a sample of nominal composition $La_6Ni_5O_{15}$ has an X-ray diffraction pattern that features reflections from two phases: $La_4Ni_3O_{10}$ and NiO. $LaNiO_2$ exists between 300 and 400°C and only under a reductive atmosphere [37].

In the La–Co–O boundary system, double oxides are thermodynamically stable phases: perovskite $LaCoO_3$ and Ruddlesden–Popper phases La_2CoO_4 and $La_4Co_3O_{10}$ [38]. All phases contain cobalt ions in various degrees of oxidation [39]. The stability of phases depends on the partial oxygen pressure and temperature. Cobalt(+3) phases have higher stability at low temperatures and at higher partial oxygen pressures. When synthesis is performed under an air atmosphere ($p(O_2)$ = 0.2 atm), $LaCoO_3$ is the only stable compound up to 1600 K.

No systematic inventions have been performed into phase equilibria in the La–Sb–O system in air. There is evidence for the existence of three compounds: La_3SbO_7, $LaSbO_4$, and $LaSb_3O_9$ [40–42]. The orthorhombic $LaSb_3O_9$ phase (space group *Cmcm*) is stable only below 1100°C and melts incongruently above this temperature to yield a $LaSbO_4$ phase [40]. $LaSbO_4$ has a monoclinic structure (space group $P2_1/m$ [43]) and exists up to 1450°C, at which temperature it decomposes to form orthorhombic La_3SbO_7 (space group *Cmcm*) [41]. The antimony in all of the above-listed compounds is antimony(+5).

In the La_2O_3–NiO–Sb_2O_3 quasi-ternary system, two ternary oxides are currently known to exist: $LaNi_{1/3}Sb_{5/3}O_6$, and $La_3Ni_2SbO_9$. $LaNi_{1/3}Sb_{5/3}O_6$ has a rosiaite-type layered structure (space group $P\bar{3}1m$) [44, 45]. Layers are formed of six-membered rings of edge-sharing (Ni/Sb)O_6 octahedra, in which Ni^{2+} and Sb^{5+} ions are arranged randomly. The La^{3+} ions reside in interlayer spaces, occupying sites on the triple axis in hexagonal-prismatic channels. The unit cell parameters of $LaNi_{1/3}Sb_{5/3}O_6$ are a = 5.26142(4) and c = 5.21945(6) Å. The compound exists up to 1050°C. At higher temperatures, it has not been studied. $La_3Ni_2SbO_9$ has a monoclinic perovskite-like structure (space group $P2_1/n$) with the unit cell parameters a = 5.0675(1), b = 5.6380(1), c = 7.9379(2) Å, β = 89.999(6)° at room temperature [46]. Two crystallographically different octahedral sites are occupied randomly by Ni^{2+} and Sb^{5+} ions. There is also evidence for the existence of $LaNi_{1-x}Sb_xO_3$ ($0 \le x \le 1/3$) limited solid solutions in the range 850–950°C. Unlike $LaNiO_3$, which has a rhombohedrally distorted perovskite structure (space group $R3c$) [47], $LaNi_{1-x}Sb_xO_3$ ($0.05 \le x \le 1/3$) solid solutions have an orthorhombically distorted perovskite structure (space group *Pbmn*), in which Ni and Sb ions are distributed randomly over the B lattice sites [48].

Only mixed oxides $LaCo_{1/3}Sb_{5/3}O_6$ [44], $La_3Co_2Sb_3O_{14}$ [49], and $La_3Co_2SbO_9$ [50], which occur in the La_2O_3–CoO–Sb_2O_5 system, are described in the literature. $LaCo_{1/3}Sb_{5/3}O_6$ is isostructural to the above-mentioned rosiaite $LaNi_{1/3}Sb_{5/3}O_6$. $La_3Co_2Sb_3O_{14}$ has a rhombohedrally distorted pyrochlore structure (space group $R\bar{3}m$, a = 7.52954(2) Å, c = 17.59983(6) Å [49]). In its crystal lattice, Co^{2+} ions occupy both the La and the Sb sites in accordance with the formula $[La_3Co'][Sb_3Co'']O_{14}$. The La, Sb, and Co ions are distributed orderly. Perovskite $La_3Co_2^{2+}Sb^{5+}O_9$ (space group $P2_1/n$) has a monoclinic structure. In $La_3Co_2^{2+}Sb^{5+}O_9$, cobalt and antimony ions occupy the same octahedral sites [50].

Therefore, the available body of data implies that the La_2O_3–(Ni/Co)O–Sb_2O_3 systems have been studied to an insufficient extent. Here, we will report the results of our study into subsolidus phase equilibria of the La_2O_3–(Ni/Co)O–Sb_2O_5 systems.

EXPERIMENTAL

The synthesis of antimonates is complicated by the high volatility of antimony. Long-term anneals at high temperatures are thereby undesirable. On the other hand, refractory precursors containing lanthanum, nickel, and cobalt react only at high temperatures. Therefore, the citrate method followed by stepwise

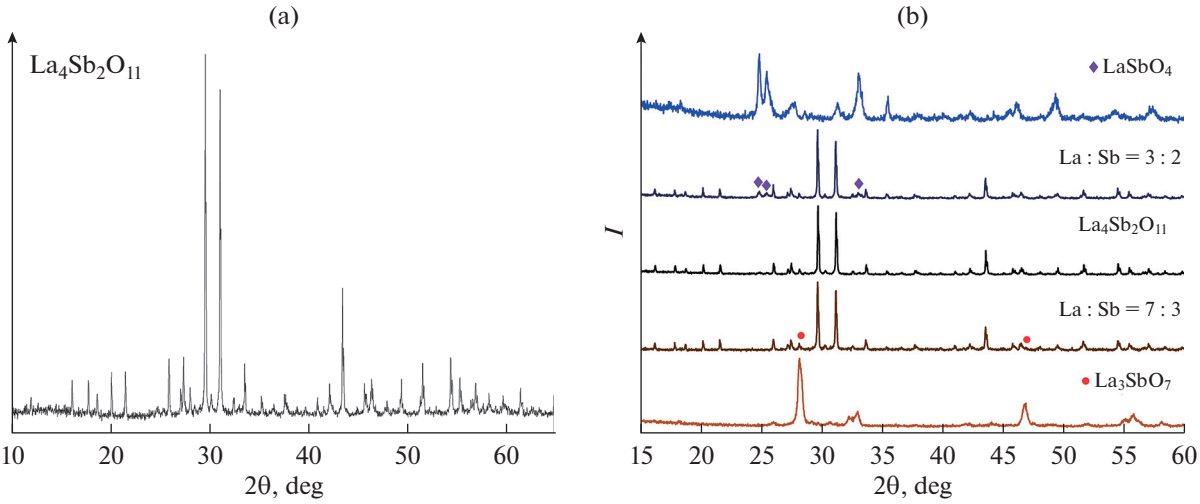

Fig. 1. (a) X-ray diffraction pattern of the $La_4Sb_2O_{11}$ phase as annealed at 1050°C and (b) X-ray diffraction patterns of samples with various La_2O_3 : Sb_2O_5 ratios. PDF 36-950 ($LaSbO_4$) and PDF 23-1138 (La_3SbO_7) were used for phase identification.

annealing was chosen to reduce the synthesis temperature. In this synthetic method, the reaction occurs at lower temperatures (compared to those of solid-phase synthesis from oxides), and the differences between the individual behaviors of cations in solution (which lead to the loss of reagents and deviation from the required composition of samples during coprecipitation synthesis) is also leveled out. Other advantages of the citrate method are a high degree of homogenization of the batch and a shorter equilibration time.

The reagents used were $La(NO_3)_3{\cdot}6H_2O$ (specialty grade), $Ni(NO_3)_2{\cdot}6H_2O$ (pure for analysis grade), $Co(NO_3)_2{\cdot}6H_2O$ (pure for analysis grade), and Sb_2O_3 (99%). Ethylene glycol $C_2H_6O_2$ (pure grade) and citric acid monohydrate (chemically pure grade) were taken in a twofold excess relative to metal ions. The components were mixed and kept in a water bath at 80°C. Dissolution of all components, thickening of the solution, and foaming were observed. After this, the reaction mixture was dried at 110°C until brittle foam formed and then pounded. The powder was first annealed at 350°C (4 h) and 450°C (4 h) to decompose the nitrates and burn out the organic components. The resulting powder was then annealed at 650 (24 h), 900 (24 h), and 1050°C (48 h) in Pt crucibles under air. The stepped annealing ensured the formation of nonvolatile intermediate products, which prevented the loss of antimony.

The phase composition of the samples was determined by X-ray powder diffraction on a Bruker D8 Advance diffractometer (CuK_α radiation, Ni filter, LYNXEYE detector). Phase identification was with reference to the PDF-2 (ICDD) database. The thermal behavior of $La_4Sb_2O_{11}$ was studied on a NETZSCH DSC 404 F1 differential scanning calorimeter. Experiments were carried out in platinum crucibles with a lid under dry argon (grade 5.5; 99.9995 vol % Ar) atmosphere at a flow rate of 10 K/min.

A diffuse reflectance spectrum in the range of 300–1100 nm was recorded on an Ocean Optics DH-2000 spectrometer equipped with an integrating sphere (50 mm ISP-50-8-R-GT). An HPX-2000 xenon lamp was used as the radiation source.

RESULTS AND DISCUSSION

As shown in the Introduction, phase equilibria in the La_2O_3–Sb_2O_5 system in air are studied insufficiently, unlike those in its La_2O_3–MO and MO–Sb_2O_5 (M = Ni or Co) boundary systems. Therefore, we considered the possibility of the existence of hitherto unknown phases in this system. A number of samples with different La_2O_3 : Sb_2O_5 ratios were synthesized, and a new compound $La_4Sb_2O_{11}$ was discovered (Fig. 1). The amount of oxygen indicated in the formula of this compound is based on the presence Sb^{5+} ions. Interplanar distances in $La_4Sb_2O_{11}$ are listed in the attachment (Table 1).

The $La_4Sb_2O_{11}$ exists up to 1060°C. The DSC heating curve in the range 1000–1500°C features three endotherm effects (Fig. 2a). The first one begins at 1060°C and corresponds to the decomposition of the $La_4Sb_2O_{11}$ phase to La_3SbO_7 and $LaSbO_4$ (Fig. 2b). The effect with the onset at 1320°C is due to incongruent melting of $LaSbO_4$ which results in the formation of a liquid phase. The presence of the liquid creates favorable conditions for the volatilization of antimony oxide; therefore, the composition of the sample upon cooling does not correspond to the original one. This explains the nonappearance of effects on the cooling curve. We have not discovered other phases that would

Table 1. Interplanar spacings for $La_4Sb_2O_{11}$

2θ, deg	*d*, Å	*I*, arb. units	*I*, %	2θ, deg	*d*, Å	*I*, arb. units	*I*, %
12.074	7.324	49	5	41.022	2.1984	33	4
16.23	5.4569	115	12	42.232	2.1381	62	7
17.878	4.9574	128	14	43.56	2.0764	227	25
18.493	4.7939	24	3	45.764	1.981	85	9
18.77	4.7236	68	7	45.948	1.9735	43	5
20.216	4.389	149	16	46.482	1.9521	30	3
21.612	4.1084	159	17	48.054	1.8918	23	2
26.029	3.4204	185	20	49.487	1.8403	52	6
27.205	3.2752	78	8	51.422	1.7758	55	6
27.489	3.2421	160	17	51.66	1.7685	185	20
28.164	3.1658	65	7	54.495	1.6828	236	26
28.596	3.119	23	2	55.416	1.6569	161	17
29.694	3.0061	921	100	56.554	1.6264	53	6
30.294	2.9479	33	4	57.011	1.6145	95	10
31.19	2.8652	822	89	58.361	1.5801	33	4
32.562	2.7476	44	5	59.025	1.5638	30	3
33.681	2.6588	116	13	59.791	1.5457	47	5
37.702	2.384	80	9	61.545	1.5058	109	12
37.713	2.3833	28	3				

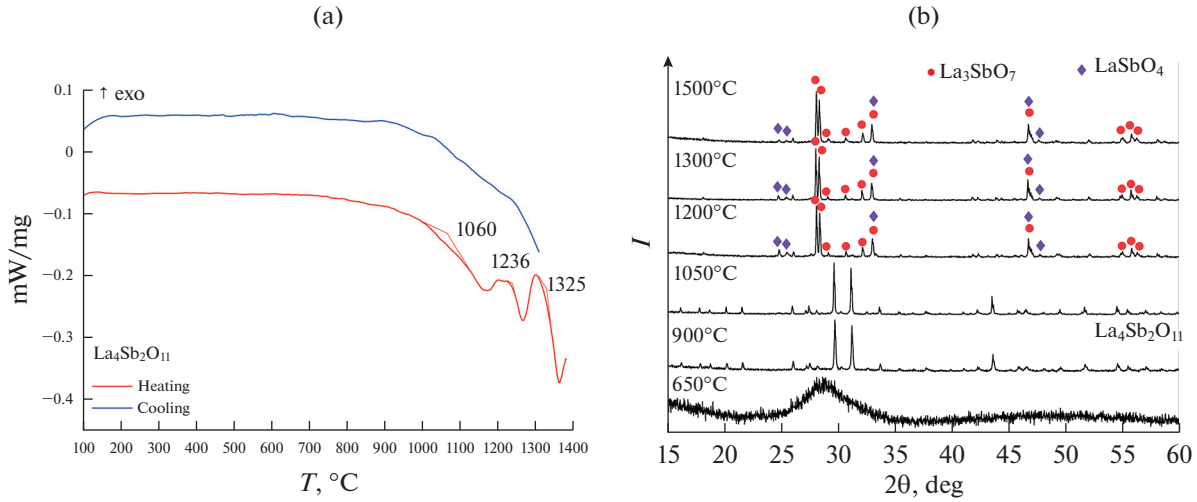

Fig. 2. (a) DSC heating and cooling curves for $La_4Sb_2O_{11}$ and (b) X-ray diffraction patterns of $La_4Sb_2O_{11}$ as-annealed at various temperatures. PDF 36-950 ($LaSbO_4$) and PDF 23-1138 (La_3SbO_7) were used for phase identification.

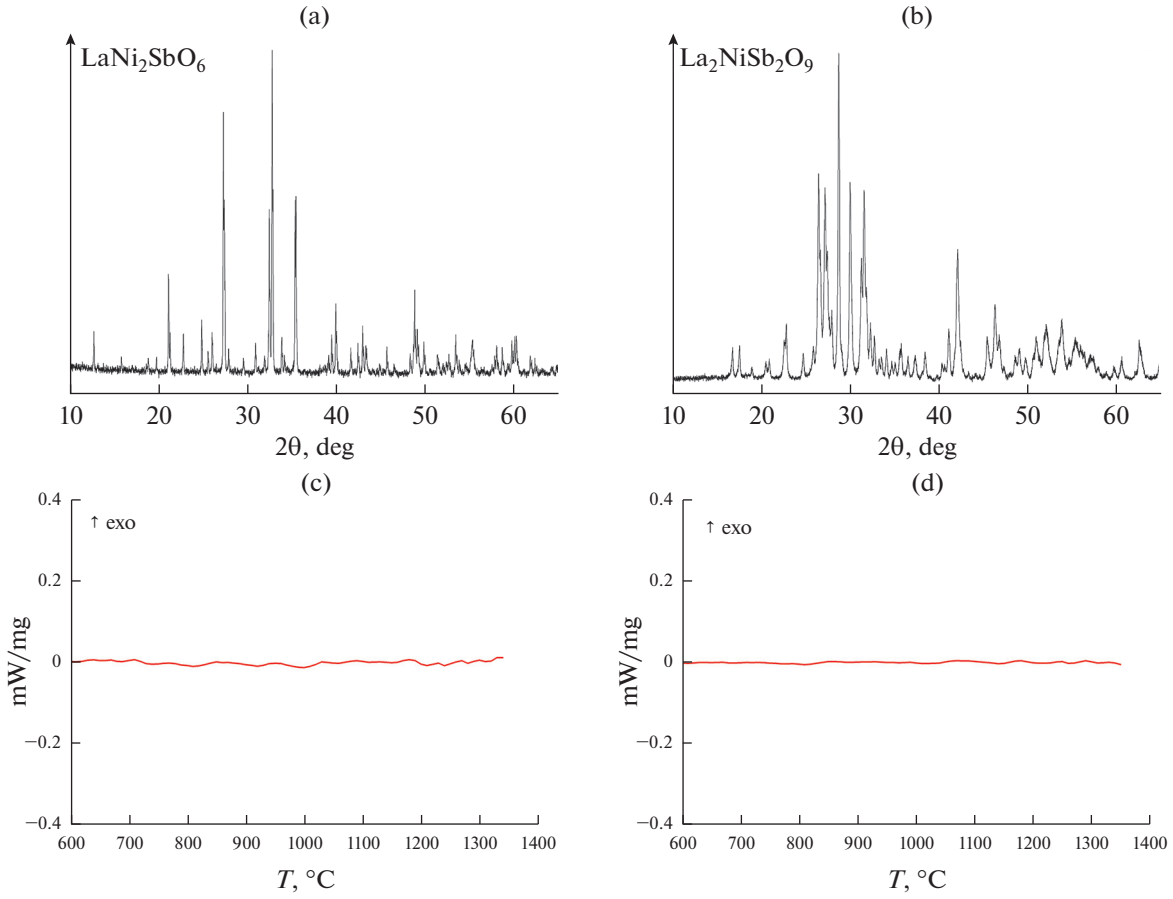

Fig. 3. (a, b) X-ray diffraction patterns and (c, d) DSC heating curves for ternary oxides: (a, c) $LaNi_2SbO_6$ and (b, d) $La_2NiSb_2O_9$.

have been previously unknown in the La_2O_3–Sb_2O_5 system.

The triangulation of the La_2O_3–(Ni/Co)O–Sb_2O_5 system at 1050°C was carried out by the cross sections methods based on XRD data.

We were the first to discover new ternary oxides in the La_2O_3–NiO–Sb_2O_5 quasi-ternary system: $LaNi_2SbO_6$ and $La_2NiSb_2O_9$ (Fig. 3; Tables 2 and 3). These compounds were stable under heating throughout the range of temperatures studied (25–1350°C). The existence of two previously known phases, namely, perovskite $La_3Ni_2SbO_9$ and rosiaite $LaNi_{1/3}Sb_{5/3}O_6$ [44–46], was verified.

The 1050°C isothermal section of the La_2O_3–NiO–Sb_2O_5 system (Fig. 4) features four ternary oxides: $LaNi_{1/3}Sb_{5/3}O_6$, $La_3Ni_2SbO_9$, $LaNi_2SbO_6$, and $La_2NiSb_2O_9$. Since the stable antimony oxide species at 1050°C in air is Sb_2O_4, the area between $LaSb_3O_9$, $NiSb_2O_6$, and antimony oxide is the projection of a more complex system: $LaSb_3O_9$–$NiSb_2O_6$–Sb_2O_3–Sb_2O_5. We have not studied the La_2O_3–NiO_x–La_3SbO_7 area in detail, as it should be regarded the projection of a quaternary system because of a mixed oxidation state of nickel in this area. We have not found new ternary oxides in the areas belonging to quaternary systems. The La_3SbO_7–NiO–$NiSb_2O_6$–$LaSb_3O_9$ section may be represented by 11 triangles of coexisting phases: La_3SbO_7–$La_3Ni_2SbO_9$–$La_4Sb_2O_{11}$, $La_4Sb_2O_{11}$–$La_3Ni_2SbO_9$–$LaSbO_4$, $La_3Ni_2SbO_9$–$LaSbO_4$–$La_2NiSb_2O_9$, $La_3Ni_2SbO_9$–$LaNi_2SbO_6$–$La_2NiSb_2O_9$, $La_3Ni_2SbO_9$–$LaNi_2SbO_6$–NiO, $LaNi_2SbO_6$–NiO–$NiSb_2O_6$, $LaNi_2SbO_6$–$LaNi_{1/3}Sb_{5/3}O_6$–$NiSb_2O_6$, $LaNi_2SbO_6$–$LaNi_{1/3}Sb_{5/3}O_6$–$La_2NiSb_2O_9$, $LaSbO_4$–$LaNi_{1/3}Sb_{5/3}O_6$–$La_2NiSb_2O_9$, $LaSbO_4$–$LaNi_{1/3}Sb_{5/3}O_6$–$LaSb_3O_9$, and $LaNi_{1/3}Sb_{5/3}O_6$–$NiSb_2O_6$–$LaSb_3O_9$.

Unlike in the nickel-containing system, three compounds have been hitherto known in the La_2O_3–CoO–Sb_2O_5 system: rosiaite $LaCo_{1/3}Sb_{5/3}O_6$, rhombohedrally distorted pyrochlore $La_3Co_2Sb_3O_{14}$, and perovskite $La_3Co_2SbO_9$ [44, 49, 50]. In addition to these compounds, we showed the existence of two more compounds, namely $La_2CoSb_2O_9$ and

Table 2. Interplanar spacings for $La_2NiSb_2O_9$

2θ, deg	*d*, Å	*I*, arb. units	*I*, %	2θ, deg	*d*, Å	*I*, arb. units	*I*, %
16.977	5.2182	45	8	33.504	2.6725	37	6
17.795	4.9803	65	11	33.774	2.6517	32	6
20.708	4.2857	46	8	34.344	2.609	53	9
21.087	4.2095	43	7	35.339	2.5378	23	4
22.795	3.8979	64	11	35.8	2.5061	35	6
23.047	3.8558	79	14	36.027	2.4909	35	6
24.96	3.5645	48	8	36.773	2.442	33	6
26.072	3.415	52	9	37.489	2.3971	48	8
26.663	3.3406	318	55	38.703	2.3246	53	9
26.91	3.3105	147	25	41.33	2.1827	47	8
27.398	3.2526	278	48	42.303	2.1347	155	27
27.671	3.2211	153	26	45.698	1.9837	84	14
28.158	3.1665	85	15	46.515	1.9507	83	14
28.945	3.0821	580	100	48.831	1.8635	39	7
30.223	2.9547	335	58	49.268	1.848	47	8
31.483	2.8393	165	28	49.978	1.8234	32	6
31.797	2.8119	237	41	51.197	1.7828	53	9
32.076	2.7881	76	13	52.039	1.7559	41	7
32.522	2.7508	60	10	53.997	1.6968	89	15
32.961	2.7152	80	14	54.025	1.696	71	12

Table 3. Interplanar spacings for $LaNi_2SbO_6$

2θ, deg	*d*, Å	*I*, arb. units	*I*, %	2θ, deg	*d*, Å	*I*, arb. units	*I*, %
12.735	6.9456	150	12	39.112	2.3016	68	5
15.831	5.5935	53	4	39.457	2.2823	165	13
18.84	4.7063	48	4	39.912	2.2574	414	33
19.756	4.4901	53	4	41.61	2.1692	113	9
21.129	4.2013	376	30	42.404	2.1302	150	12
22.781	3.9002	138	11	42.929	2.1054	240	19
24.844	3.5808	179	14	43.268	2.0896	115	9
25.561	3.482	74	6	44.829	2.0202	63	5
27.265	3.2681	890	70	45.657	1.9857	136	11
27.383	3.2544	470	37	46.502	1.9513	47	4
27.86	3.1997	67	5	48.266	1.8844	97	8
29.544	3.0221	47	4	48.63	1.8708	118	9
30.883	2.8934	108	9	48.772	1.8658	385	30
31.898	2.8032	44	3	49.08	1.8549	245	19
32.441	2.758	265	21	49.809	1.8294	169	13
32.764	2.7315	1269	100	51.343	1.7781	93	7
33.841	2.6478	188	15	53.389	1.7147	178	14
35.343	2.5382	949	75	53.768	1.7035	71	6
35.435	2.5377	490	39	55.275	1.6605	74	6

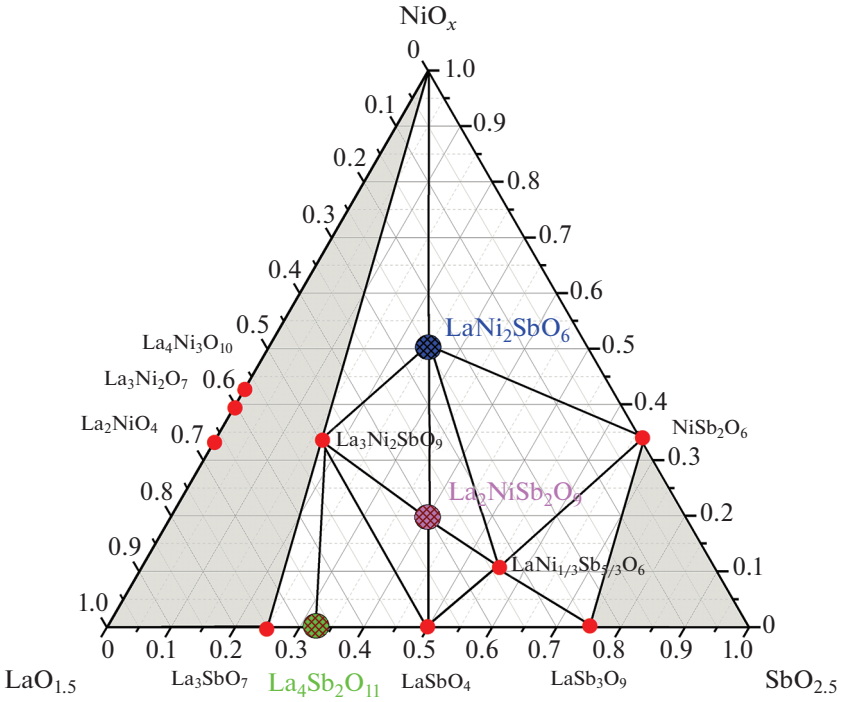

Fig. 4. 1050°C isothermal section of the La_2O_3–NiO–Sb_2O_5 system.

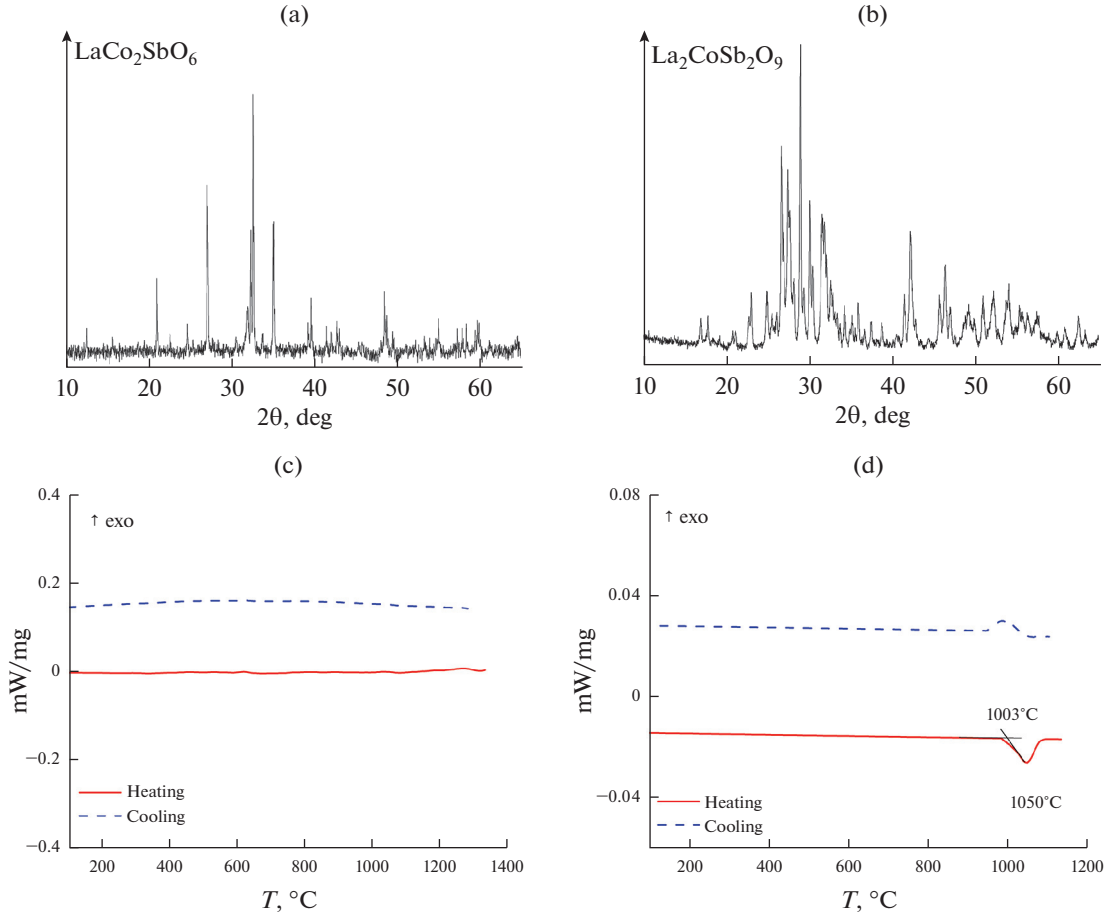

Fig. 5. (a, b) X-ray diffraction patterns and (c, d) DSC curves of new ternary oxides: (a, c) $LaCo_2SbO_6$ and (b, d) $La_2CoSb_2O_9$.

Table 4. Interplanar spacings for $La_2CoSb_2O_9$

2θ, deg	*d*, Å	*I*, arb. units	*I*, %	2θ, deg	*d*, Å	*I*, arb. units	*I*, %
17.012	5.2077	58	8	33.429	2.6782	54	7
17.832	4.9699	63	8	33.762	2.6526	43	6
20.813	4.2644	35	5	34.304	2.6119	78	10
21.186	4.1902	30	4	35.206	2.547	50	7
22.792	3.8984	49	6	35.553	2.523	26	3
23.09	3.8488	128	17	35.952	2.4959	99	13
24.954	3.5653	91	12	36.722	2.4453	29	4
25.57	3.4808	32	4	37.526	2.3947	56	7
26.146	3.4054	51	7	38.799	2.3191	44	6
26.7	3.336	410	54	41.465	2.1759	111	15
27.471	3.2441	279	37	42.244	2.1376	186	24
27.779	3.2089	192	25	45.684	1.9843	79	10
28.187	3.1633	124	16	46.43	1.9541	142	19
28.996	3.0769	788	104	48.789	1.865	77	10
30.49	2.9294	178	23	49.155	1.852	94	12
31.589	2.83	162	21	49.899	1.8261	31	4
31.903	2.8028	132	17	50.992	1.7895	69	9
32.155	2.7815	128	17	52.032	1.7561	130	17
32.602	2.7443	78	10	53.998	1.6967	143	19
32.895	2.7205	67	9	55.376	1.6577	48	6

$LaCo_2SbO_6$, which are isostructural to those found in the nickel system (Fig. 5; Tables 4 and 5). $LaCo_2SbO_6$ is stable over the entire range of investigation up to 1350°C. $La_2CoSb_2O_9$, unlike its isostructural nickel analogue, decomposes at 1003°C. In the La_2O_3–CoO_x–La_3SbO_7 area, no ternary oxides have been found. Therefore, the 1050°C isothermal section of the La_2O_3–CoO–Sb_2O_5 system in the La_3SbO_7–CoO–$LaSb_3O_9$–$CoSb_2O_6$ area may be represented by 14 triangles of coexisting phases (Fig. 6): La_3SbO_7–$La_3Co_2SbO_9$–$La_4Sb_2O_{11}$, $La_4Sb_2O_{11}$–$La_3Co_2SbO_9$–$La_3Co_2Sb_3O_{14}$, $La_3Co_2Sb_3O_{14}$–$La_4Sb_2O_{11}$–$La_2CoSb_2O_9$, $La_4Sb_2O_{11}$–$La_2CoSb_2O_9$–$LaSbO_4$, $La_3Co_2SbO_9$–$La_3Co_2Sb_3O_{14}$–$LaCo_2SbO_6$, $La_3Co_2SbO_9$–

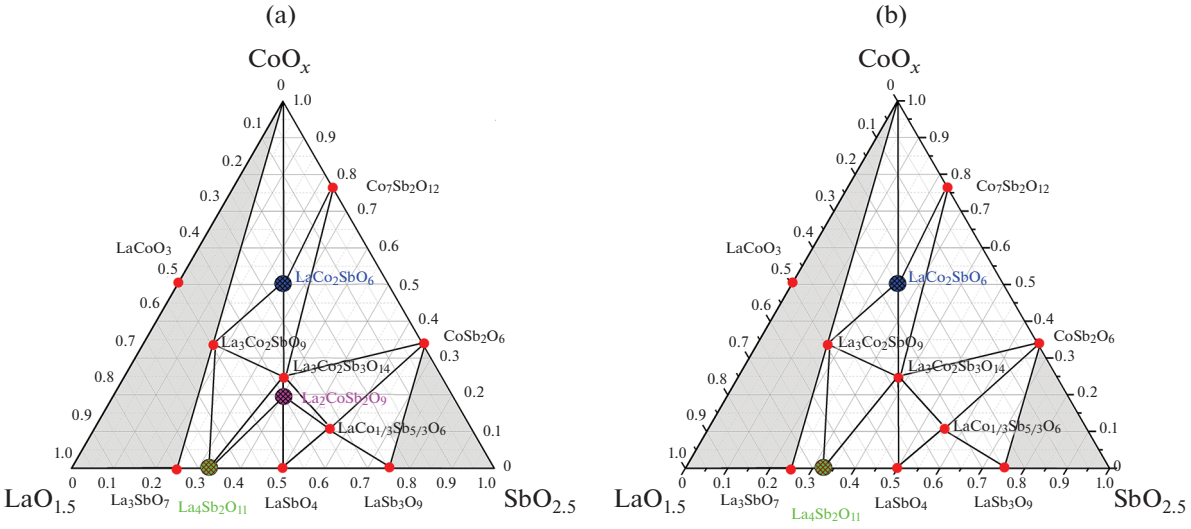

Fig. 6. (a) 900 and (b) 1050°C isothermal sections of the La_2O_3–CoO–Sb_2O_5 system.

Table 5. Interplanar spacings for $LaCo_2SbO_6$

2θ, deg	*d*, Å	*I*, arb. units	*I*, %	2θ, deg	*d*, Å	*I*, arb. units	*I*, %
12.733	6.9464	120	5	39.013	2.3068	53	2
15.854	5.5852	67	3	39.357	2.2876	155	7
18.848	4.7043	52	2	39.718	2.2677	482	21
19.674	4.5086	30	1	41.526	2.1727	105	5
21.123	4.2026	358	16	42.185	2.1406	172	8
22.751	3.9064	155	7	42.814	2.1106	233	10
24.853	3.5809	249	11	43.119	2.0961	142	6
25.466	3.4955	101	4	44.625	2.0289	42	2
27.189	3.279	1529	67	45.485	1.9925	73	3
27.261	3.2686	780	34	46.38	1.9561	37	2
27.842	3.2017	63	3	48.114	1.8896	63	3
29.363	3.0393	79	3	48.426	1.8782	142	6
30.71	2.9089	112	5	48.562	1.8731	506	22
31.846	2.8077	49	2	48.833	1.8634	232	10
32.451	2.7572	778	34	49.567	1.8377	137	6
32.733	2.7342	2277	100	51.127	1.7851	48	2
33.838	2.6469	127	6	53.332	1.7162	132	6
35.145	2.5515	1114	49	53.651	1.7069	65	3
35.234	2.5451	796	35	55.074	1.6662	169	7

$LaCo_2SbO_6$–CoO, $LaCo_2SbO_6$–CoO–$Co_7Sb_2O_{12}$, $LaCo_2SbO_6$–$Co_7Sb_2O_{12}$–$La_3Co_2Sb_3O_{14}$, $Co_7Sb_2O_{12}$–$La_3Co_2Sb_3O_{14}$–$CoSb_2O_6$, $La_3Co_2Sb_3O_{14}$–$CoSb_2O_6$–$LaCo_{1/3}Sb_{5/3}O_6$, $La_3Co_2Sb_3O_{14}$–$La_2CoSb_2O_9$–$LaCo_{1/3}Sb_{5/3}O_6$, $La_2CoSb_2O_9$–$LaSbO_4$–$LaCo_{1/3}Sb_{5/3}O_6$, $LaSbO_4$–$LaCo_{1/3}Sb_{5/3}O_6$–$LaSb_3O_9$, and $LaCo_{1/3}Sb_{5/3}O_6$–$LaSb_3O_9$–$CoSb_2O_6$.

The diffuse reflectance optical spectra of the new phases (Fig. 7) confirmed that nickel and cobalt are in the +2 oxidation state. The spectrum of octahedrally coordinated Ni^{2+} is known to feature three allowed *d*–*d* transitions from the $^3A_{2g}$ ground level to $^3T_{2g}$, $^3T_{1g}$, and $^3T_{1g}(P)$ [51]. In oxides, bands corresponding to these transitions appear in the ranges 7000–10000,

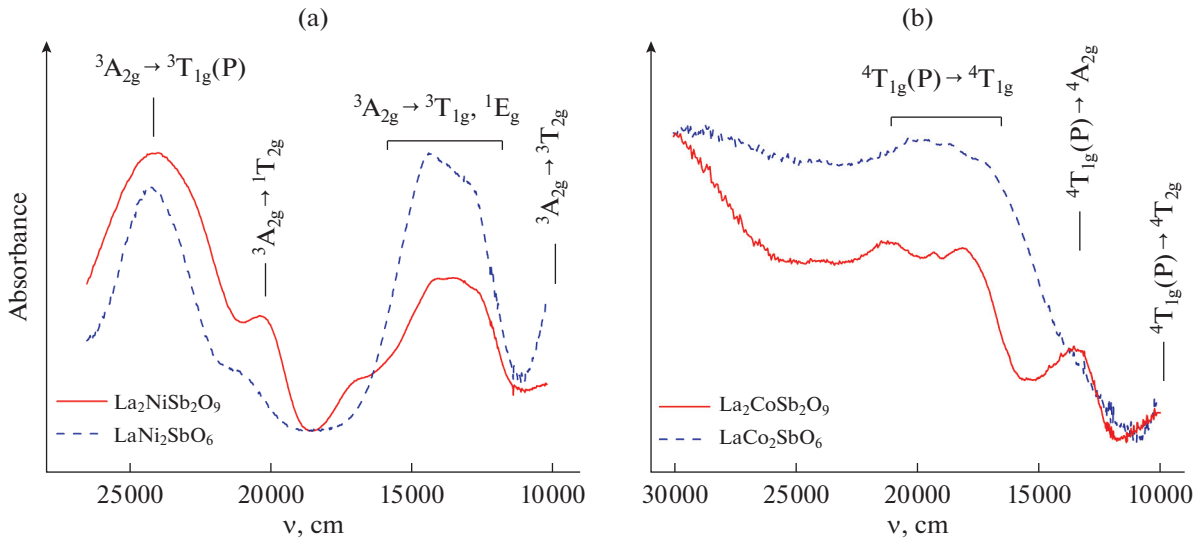

Fig. 7. Diffuse reflectance spectra in the visible of (a) $LaNi_2SbO_6$, and $La_2NiSb_2O_9$ and (b) $LaCo_2SbO_6$ and $La_2CoSb_2O_9$.

12000–16000, and 22000–27000 cm^{-1}. Bands associated with $^3A_{2g} \rightarrow {}^1E_g$ and $^3A_{2g} \rightarrow {}^1T_{2g}$ spin-forbidden transitions can also be observable. The ^1E_g and $^3T_{1g}$ states are close in energy to each other. As a result of spin–orbit coupling, the $^3A_{2g} \rightarrow {}^1E_g$ forbidden transition grows in intensity due to the allowed transition, so a doublet appears in Ni^{2+} spectra in the range 12000–16000 cm^{-1}. The $^3A_{2g} \rightarrow {}^1T_{2g}$ spin-forbidden transition usually appears as a weak band at the long-wavelength edge of the $^3A_{2g} \rightarrow {}^3T_{1g}$ transition. All the above-listed features appear in the $LaNi_2SbO_6$, $La_2NiSb_2O_9$, and $LaNi_{1/3}Sb_{5/3}O_6$ spectra (Fig. 7). $LaNi_{1/3}Sb_{5/3}O_6$ is shown as a reference. This indicates that nickel ions in these compounds are in the +2 oxidation state.

The spectra of octahedrally coordinated Co^{2+} usually feature two strong bands in the ranges 8000–10000 and 16 000–20 000 cm^{-1} referring to $^4T_{1g}(P) \rightarrow {}^4T_{2g}$ and $^4T_{1g}(P) \rightarrow {}^4T_{1g}$ allowed transitions, respectively [51]. The $^4T_{1g}(P) \rightarrow {}^4T_{1g}$ band, as a rule, is a multiplet due to an admixture of spin-forbidden transitions. In the range 11000–14000 cm^{-1}, a less strong $^4T_{1g}(P) \rightarrow {}^4A_{2g}$ transition is observed; it frequently appears as a shoulder at the low-energy side of the $^4T_{1g}(P) \rightarrow {}^4T_{1g}$ transition band. The $LaCo_2SbO_6$ and $La_3Co_2SbO_9$ spectra, just as the $La_3Co_2Sb_3O_{14}$ spectrum given as a reference, have all the listed features, indicating the presence of Co^{2+} ions in an octahedral surrounding in these compounds. The different degrees of splitting of the observed transitions are explained by the structural specifics of the compounds.

Therefore, the fact that the nickel and cobalt are Ni^{2+} and Co^{2+} in all the prepared ternary oxides, implies that, indeed, the above-considered La_3SbO_7–NiO–$NiSb_2O_6$–$LaSb_3O_9$ and La_3SbO_7–CoO–$LaSb_3O_9$–$CoSb_2O_6$ areas belong to the La_2O_3–NiO–Sb_2O_5 and La_2O_3–CoO–Sb_2O_5 systems, respectively.

CONCLUSIONS

Altogether, the La_2O_3–$(Ni/Co)O$–Sb_2O_5 systems are not completely alike. They implement four pairs of isostructural compounds: $La(Ni/Co)_{1/3}Sb_{5/3}O_6$, $La_3(Ni/Co)_2SbO_9$, $La(Ni/Co)_2SbO_6$, and $La_2(Ni/Co)Sb_2O_9$; in the cobalt oxide system, however, one more compound exists: $La_3Co_2SbO_9$. The above-listed compounds differ from one another in $(Ni/Co)^{2+}/Sb^{5+}$ cation ratios and have different structures. The known ternary oxides were characterized previously. Some of them were shown to have functional properties that allowed them to be considered promising for use. For example, the rosiaite compound $LaNi_{1/3}Sb_{5/3}O_6$ exhibited high catalytic activity in CO oxidation [20]. Therefore, a further study of the new phases first synthesized in this work would be of undoubted interest.

ACKNOWLEDGMENTS

Facilities of the Shared Facilities Center of the Kurnakov Institute were used to fulfill the work.

FUNDING

This work was supported by the Russian Science Foundation (project No. 23-23-00113).

CONFLICT OF INTEREST

The authors declare that they have no known competing financial interests or personal relationships that could have appeared to influence the work described in this article.

REFERENCES

1. J. Sato, N. Saito, H. Nishiyama, et al., J. Photochem. Photobiol., A **148**, 85 (2002). https://doi.org/10.1016/S1010-6030(02)00076-X
2. I. A. Moreno-Hernandez, B. S. Brunschwig, and N. S. Lewis, Energy Environ. Sci. **12**, 1241 (2019). https://doi.org/10.1039/C8EE03676D
3. G. K. K. Gunasooriya, M. E. Kreider, Y. Liu, et al., ACS Nano **16**, 6334 (2022). https://doi.org/10.1021/acsnano.2c00420
4. I. A. Moreno-Hernandez, C. A. MacFarland, C. G. Read, et al., Energy Environ. Sci. **10**, 2103 (2017). https://doi.org/10.1039/C7EE01486D
5. L. Zhou, A. Shinde, J. H. Montoya, et al., ACS Catal. **8**, 10938 (2018). https://doi.org/10.1021/acscatal.8b02689
6. T. A. Evans and K.-S. Choi, ACS Appl. Energy Mater. **3**, 5563 (2020). https://doi.org/10.1021/acsaem.0c00526
7. K. Ham, S. Hong, S. Kang, et al., ACS Energy Lett. **6**, 364 (2021). https://doi.org/10.1021/acsenergylett.0c02359
8. L. Zhou, Y. Wang, K. Kan, et al., ACS Sustainable Chem. Eng. **10**, 15898 (2022). https://doi.org/10.1021/acssuschemeng.2c05239
9. M. M. Gadgil and S. K. Kulshreshtha, J. Mol. Catal. A: Chem. **95**, 211 (1995). https://doi.org/10.1016/1381-1169(94)00027-1
10. M. Karimi, S. Dariush, A. Kobra, et al., Tetrahedron Lett. **56**, 2674 (2015). https://doi.org/10.1016/j.tetlet.2015.03.114
11. R. K. Grasselli, J. Chem. Educ. **63**, 216 (1986). https://doi.org/10.1021/ed063p216
12. N. Burriesci, F. Garbassi, M. Petrera, et al., J. Chem. Soc., Faraday Trans. **78**, 817 (1982). https://doi.org/10.1039/F19827800817
13. R. G. Teller, J. F. Brazdil, R. K. Grasselli, et al., J. Chem. Soc., Faraday Trans. **81**, 1693 (1985). https://doi.org/10.1039/F19858101693

14. A. V. Egorysheva, O. G. Ellert, and E. Yu. Liberman, J. Alloys Compd. **777**, 655 (2019). https://doi.org/10.1016/j.jallcom.2018.11.008
15. O. G. Ellert, A. V. Egorysheva, and E. Yu. Liberman, Inorg. Mater. **55**, 1257 (2019). https://doi.org/10.1134/S0020168519120033
16. E. Yu. Liberman, O. G. Ellert, A. V. Naumkin, et al., Russ. J. Inorg. Chem. **65**, 592 (2020). https://doi.org/10.1134/S0036023620040117
17. O. G. Ellert, A. V. Egorysheva, E. Yu. Liberman, et al., Ceram. Int. **46**, 27725 (2020). https://doi.org/10.1016/j.ceramint.2020.07.271
18. A. V. Egorysheva, O. G. Ellert, E. Yu. Liberman, et al., Russ. J. Inorg. Chem. **67**, 2127 (2022). https://doi.org/10.1134/S0036023622601349
19. A. V. Egorysheva, K. R. Plukchi, S. V. Golodukhina, et al., Mendeleev Commun. **33**, 608 (2023). https://doi.org/10.1016/j.mencom.2023.09.005
20. A. V. Egorysheva, S. V. Golodukhina, K. R. Plukchi, et al., Russ. J. Inorg. Chem **68**, 1725 (2023). https://doi.org/10.1134/S0036023623602106
21. K. Swaminathan and O. M. Sreedharan, J. Alloys Compd. **292**, 100 (1999). https://doi.org/10.1016/S0925-8388(99)00283-2
22. H. Haeuseler, Spectrochim. Acta, Part A **37**, 487 (1981). https://doi.org/10.1016/0584-8539(81)80036-0
23. H. Ehrenberg, G. Wltschek, J. Rodriguez-Carvajal, et al., J. Magn. Magn. Mater. **184**, 111 (1998). https://doi.org/10.1016/S0304-8853(97)01122-0
24. V. M. Rodríguez-Betancourtt, H. G. Bonilla, M. F. Martínez, et al., J. Nanomater **2017**, 8792567 (2017). https://doi.org/10.1155/2017/8792567
25. A. Singh, A. Singh, S. Singh, et al., Chem. Phys. Lett. **646**, 41 (2016). https://doi.org/10.1016/j.cplett.2016.01.005
26. A. Y. Nikulin, E. A. Zvereva, V. B. Nalbandyan, et al., Dalton Trans. **46**, 6059 (2017). https://doi.org/10.1039/C6DT04859E
27. J. R. Gavarri, R. Chater, and J. Ziolkowski, J. Solid State Chem. **73**, 305 (1988). https://doi.org/10.1016/0022-4596(88)90114-4
28. J. P. Turbil and J. C. Bernier, C. R. Acad. Sci., Ser. C **227**, 1347 (1973).
29. P. Odier, Y. Nigara, J. Coutures, et al., J. Solid State Chem. **56**, 32 (1985). https://doi.org/10.1016/0022-4596(85)90249-X
30. M. S. L. Brito, M. T. Escote, C. O. P. Santos, et al., Mater. Chem. Phys. **88**, 404 (2004). https://doi.org/10.1016/j.matchemphys.2004.08.008
31. H. D. Zhou, C. R. Wiebe, J. A. Janik, et al., J. Solid State Chem. **183**, 890 (2010). https://doi.org/10.1016/j.jssc.2010.01.025
32. K. Kitayama, J. Solid State Chem. **87**, 165 (1990). https://doi.org/10.1016/0022-4596(90)90078-C
33. R. A. M. Ram, L. Ganapathi, P. Ganguly, et al., J. Solid State Chem. **63**, 139 (1986). https://doi.org/10.1016/0022-4596(86)90163-5
34. A. Wold, B. Post, and E. Banks, J. Am. Chem. Soc. **79**, 4911 (1957). https://doi.org/10.1021/ja01575a022
35. M. Zinkevich and F. Aldinger, J. Alloys Compd. **375**, 147 (2004). https://doi.org/10.1016/j.jallcom.2003.11.138
36. A. N. Demina, V. A. Cherepanov, A. N. Petrov, et al., Inorg. Mater. **41**, 736 (2005). https://doi.org/10.1007/s10789-005-0201-2
37. M. A. Hayward, M. A. Green, M. J. Rosseinsky, et al., J. Am. Chem. Soc. **121**, 8843 (1999). https://doi.org/10.1021/ja991573i
38. W.-W. Zhang, E. Povoden-Karadeniz, H. Xu, et al., J. Phase Equilib. Diff. **40**, 219 (2019). https://doi.org/10.1007/s11669-019-00717-z
39. Y. Adachi, N. Hatada, and T. Uda, J. Electrochem. Soc. **163**, F1084 (2016). https://doi.org/10.1149/2.0811609je
40. K. M. Ok, A. Gittens, L. Zhang, et al., J. Mater. Chem. **14**, 116 (2004). https://doi.org/10.1039/B307496J
41. K. P. F. Siqueira, R. M. Borges, E. Granado, et al., J. Solid State Chem. **203**, 326 (2013). https://doi.org/10.1016/j.jssc.2013.05.001
42. M. B. Varfolomeev, T. A. Toporenskaya, and V. V. Burlyaev, Russ. J. Inorg. Chem. **26**, 171 (1981).
43. K. P. F. Siqueira, R. M. Borges, J. C. Soares, et al., Mater. Chem. Phys. **140**, 255 (2013). https://doi.org/10.1016/j.matchemphys.2013.03.031
44. G. Blasse and A. D. M. De Pauw, J. Inorg. Nucl. Chem. **32**, 2533 (1970). https://doi.org/10.1016/0022-1902(70)80298-6
45. O. G. Ellert, A. V. Egorysheva, S. V. Golodukhina, et al., Russ. Chem. Bull. **70**, 2397 (2021). https://doi.org/10.1007/s11172-021-3359-0
46. P. D. Battle, S. I. Evers, E. C. Hunter, et al., Inorg. Chem. **52**, 6648 (2013). https://doi.org/10.1021/ic400675r
47. I. Alvarez, M. L. Veiga, and C. Pico, Solid State Ionics **91**, 265 (1996). https://doi.org/10.1016/S0167-2738(96)83028-1
48. I. Alvarez, M. L. Veiga, and C. Pico, J. Alloys Compd. **255**, 74 (1997). https://doi.org/10.1016/S0925-8388(96)02870-8
49. K. Li, Y. Hu, Y. Wang, et al., J. Solid State Chem. **217**, 80 (2014). https://doi.org/10.1016/j.jssc.2014.05.003
50. D. G. Franco, V. C. Fuertes, M. C. Blanco, et al., J. Solid State Chem. **194**, 385 (2012). https://doi.org/10.1016/j.jssc.2012.05.045
51. A. B. P. Lever, *Inorganic Electronic Spectroscopy*, vol. 2 (Elsevier, 1984).

Translated by O. Fedorova